Identification of New Inhibitors for *Klebsiella Pneumoniae* Trimethoprim-Resistant Dihydrofolate Reductase: An i*n Silico* Drug Repurposing Study

Mostafa Khedrinia
Golestan University
Farzad Khademi
Ardabil University of Medical Sciences: Ardebil University of Medical Sciences
Seyed Ali Mirhosseini
Baqiyatallah University of Medical Sciences
Ramezan Ali Taheri (r.a.taheri@gmail.com)
Baghiatollah University of Medical Sciences: Baqiyatallah University of Medical Sciences
https://orcid.org/0000-0003-1394-6412

Research Article

Keywords: Klebsiella pneumoniae, Dihydrofolate reductase, Drug repurposing, Docking, Molecular dynamics simulation

Posted Date: November 2nd, 2021

DOI: https://doi.org/10.21203/rs.3.rs-908683/v1

Abstract

Klebsiella pneumoniae is a gram-negative, non-motile, rod-shaped, and pathogenic bacterium that is widely mutated and resistant to antibiotics. It can cause a wide range of hospital infections such as pneumonia, urinary tract infection, and blood-stream infection in humans. Identification and development of potential drugs due to high drug resistance by *Klebsiella pneumoniae* are inevitable. Dihydrofolate reductase is a vital enzyme for cells because it converts 7,8-dihydrofolate to 5,6,7,8-tetrahydrofolate. Trimethoprim (TMP) is an inhibitor of *K. pneumoniae* DHFR and other micro-organisms, but resistance to its action develops quickly when it is used. Identifying and designing new drugs is a costly, time-consuming, and challenging process. On the other hand, computational drug repurposing has become an efficient, economical and riskless strategy. In this study, the structure-based virtual docking approach was used to screen the FDA-approved drugs data-set against *K. pneumoniae* trimethoprim-resistance DHFR to identify potential hit compounds. Then, to validate the hit compounds, molecular dynamics simulations and MM/PBSA analyses were carried out. Our computational drug repurposing results show that the Olodaterol and Pazopanib like reference ligand interact with key residues such as Ile20, Glu27, Phe31, Met50, Leu53 and inhibit *K. pneumoniae* trimethoprim-resistant dihydrofolate reductase while TMP does not have strong interaction with the active site. According to the results of the current study and since it was based on drug repurposing both compounds of Pazopanib and Olodaterol could be evaluated in phase 2 clinical trials.

1. Introduction

For nearly a century, antibiotics have been used continuously to treat bacterial infections. The consequence of this trend is the resistance of bacteria, especially the *Enterobacteriaceae* family which has become a global medical crisis (Navon-Venezia et al., 2017). Two mechanisms of genetic and mechanistic basis such as horizontal gene transfer, modification of antibiotic molecule, change in the target site, and decreased antibiotic penetration are the main reasons for the resistance of bacteria to antibiotics (Munita et al., 2016). One of the most mutable and antibiotic-resistant bacteria is *Klebsiella pneumoniae*. It is a gram-negative, non-motile, encapsulated, lactose-fermenting, facultative anaerobic, rod-shaped, and pathogenic bacteria that naturally exist in the mouth, nose, and throat and on the skin (Doorduijn et al., 2016; Kidd et al., 2017; Li et al., 2014). Naturally, *K. pneumoniae* is not a pathogenic organism in humans but, in the case of aspiration, it can damage the lung alveoli and causes dangerous pneumonia. It can make a wide range of hospital infections such as pneumonia (Prince, S. E., Dominger, K. A., Cunha, B. A., Klein, N. C., Brook, M., Brook, 2000), urinary tract infection (El Bouamri et al., 2015), wound infection (Chung, 2016), thrombophlebitis (Maffiolo et al., 2006), osteomyelitis (Sanders, 1989), meningitis (Fang et al., 2000), cholecystitis (Capoor et al., 2008), sepsis and blood-stream infection (Girometti et al., 2014) in humans and these infections are worse in children, the elderly, people with the weak immune system and alcoholism (Kidd et al., 2017). Many antibiotics are used to inhibit the activity of *K. pneumoniae*, the most important of which are ampicillin/sulbactam, piperacillin/tazobactam, ceftazidime, cefepime, levofloxacin, norfloxacin, gatifloxacin, moxifloxacin, and ciprofloxacin (Brisse et

al., 1999; Hawser et al., 2011; Hoffman et al., 1992). However, the ability of this organism to counteract antibiotics due to having a wide range of beta-lactamases and carbapenemases is high, as far as some strains isolated in the clinic are resistant to all antibiotics and the treatment of them are very difficult (Brolund et al., 2010; Hirsch et al., 2011). *K. pneumoniae* resistance to antibiotics has several consequences, including increased mortality, hospitalization, and cost, and according to the World Health Organization (WHO) statement, pneumonia is one of the most important multidrug-resistant (MDRs) diseases that threatens human health (Kidd et al., 2017; Navon-Venezia et al., 2017).

Nowadays, various enzymes including proteases, topoisomerases, transferases, hydrolases, and reductases are targeted to control and treat pathogenic bacteria. Dihydrofolate reductase (DHFR) is one of the most important and validated targets which exists in all cells and, on the other hand, it has a special structure in different species that makes it suitable for designing potent and selective inhibitors (Lamb et al., 2014). Dihydrofolate reductase catalyzes the reduction of 7,8-dihydrofolate (DHF) to 5,6,7,8-tetrahydrofolate (THF) using coenzyme NADPH and the proton of water molecule respectively as the donor of the hydride ion. The mechanism of enzyme catalysis and the role of individual amino acids in the reaction has always been extensively studied by experimental and quantum chemical methods. The catalytic process involves two steps protonation of dihydrofolate at N5 atom and transfer of hydride ion to positively charged intermediate. This is done with the help of the aspartic acid in prokaryotes. The rate of transfer of hydride ion to the substrate is the key stage of the catalytic process. It was found that the reduction of 7, 8- Dihydrofolate was accompanied by the transfer of hydrogen atom located in 4-pro R position of NADPH to C-6 atom of dihydrofolate. In the end, NADPH is oxidized to NADP + and 5,6,7,8-tetrahydrofolate is produced. The tetrahydrofolate and its metabolites are involved in the biosynthesis of thymidine monophosphate (dTMP), purine bases, and methionine. Due to the role of dihydrofolate reductase in the production of DNA and RNA precursors, inhibition of the enzyme in the S-phase cells reduces the level of tetrahydrofolate, which eventually leads to cell death (Rao & Road, 2013)·(H. Wang et al., 2016).

Trimethoprim (TMP) is an inhibitor of DHFR of *K. pneumoniae* and other micro-organisms. It is usually used in combination with other antibiotics(Lombardo et al., 2016). The combination of trimethoprim-sulfamethoxazole (TMP/SMX) is generally well tolerated but can induce adverse effects such as leukopenia, thrombocytopenia (Gordin, 1984), anemia (Ho & Juurlink, 2011), agranulocytosis, evocative of a disorder of cellular maturation, probably secondary to an inhibition of the human DHFR (Wu et al., 2015). This combination can cause severe but rare dermatological reactions, Stevens-Johnson and Lyell syndromes (Rijal et al., 2014). Trimethoprim can also cause hyperkalemia by decreasing urinary potassium elimination (Nickels et al., 2012; Velázquez et al., 1993). Resistance to antibiotics has prompted researchers to always look for compounds to control pathogenic bacteria. On the other hand, the long-term use of trimethoprim against the *K. pneumonia* infection has caused some of its strains to encode a TMP-resistant DHFR by expression of the DfrA1 gene (Lam et al., 2014). Mutations in Asp27 and Leu28 to Glu and Gln, Ile50 to Met50 and Ile94 to Ser, and also deletion of proline between residues 54 – 49, reduces the affinity of the DHFR to trimethoprim (Lombardo et al., 2016).

Structure-based drug discovery (SBDD) is a rapidly rising method in molecular biology and drug design. The purpose of this method is to investigate the mechanism of inhibition and activation of different targets at the atomic scale. Designing and developing new drugs for molecular targets is a time-consuming and costly process. On the other hand, drug repurposing is a process to find existing drugs for a novel medical indication. Each of these two methods (SBDD and drug repurposing) has been very successful in introducing new drugs(Batool et al., 2019; Naveja et al., 2011). Computational drug repurposing approach saves cost and time in drug discovery and also the drugs used in this method have known pharmacokinetics and safety profiles. In recent years, computational methods have always been of interest to researchers. In humans, DHFR is a potential target for cancer treatment, and many studies have been conducted on it, both in the field of computational(Rana et al., 2019) and experimental(Kubbies & Stockinger, 1990). Many studies have also been performed to identify new drugs for pathogenic parasitic(Anderson, 2005) and bacterial dihydrofolate reductase, including leishmania donovani(Vadloori et al., 2018), Toxoplasma gondii(Pacheco Homem et al., 2013), and Yersinia pestis(Bastos et al., 2016), using computational methods. On the other hand, no research has been done in this field on Klebsiella pneumoniae trimethoprim-resistant dihydrofolate reductase (DfrA1). Herein, we intend to identify novel inhibitors for the DfrA1 from FDA-approved drugs library using molecular modeling methods such as Structure-Based Virtual Screening (SBVS), Molecular Dynamics (MD) and binding free energy calculations (MMPBSA).

2. Material And Methods

2.1. Ligand and receptor preparation

K. pneumoniae trimethoprim-resistant dihydrofolate reductase has two crystallographic structures in Protein Data Bank (PDB) (Gohlke et al., 2000). The first structure, 5ECX has a resolution of 1.95 Å and is complexed with NADPH and 6-ethyl-5-(3-(6-(pyridin-4-yl) benzo[d] [1, 3] dioxol-4-yl) but-1-yn-1-yl) pyrimidine-2, 4-diamine (5N1), and the second one, 5ECC has a resolution of 1.87 Å and co-crystallized with NADPH and 6-ethyl-5-(3-(2-methoxy-5-(pyridin-4-yl) phenyl) prop-1-yn-1-yl) pyrimidine-2, 4-diamine (6DR) (Lombardo et al., 2016). The 5ECC was selected as the target structure for molecular docking because it has a better resolution than 5ECX. The two-dimensional structure of FDA-approved drugs was obtained from the DrugBank database (Version 5.1.2) and was converted into 3D by the Molconverter software. Additional coordinates, for example, co-crystallized ligand and crystallographic waters were removed from 5ECC, and then polar hydrogen atoms were added and Kollman charges and atomic solvation parameters were assigned to the target protein. Parallelly Gasteiger partial charges were added to the ligands. All of these steps were done by the UCSF Chimera and AutoDock Tools software.

2.2. Structure-Based Virtual Screening

Molecular docking between DfrA1 and small molecules library was performed by the AutoDock Vina software using the Lamarckian Genetic Algorithm (LGA). To define the binding site, we selected the co-crystallized ligand as the center of the binding pocket with 22.88, -18.42, -0.39 coordinates, and also the

most important residue was identified from binding pocket, which has some essential interactions with the substrate. The grid box volume was set to 38×38×38 points with a grid spacing of 0.375Å. In addition, the FDA-approved drugs, reference ligand (6DR), and trimethoprim also were docked with DfrA1 as a positive and negative control, respectively.

In the first step, 100 compounds with the lowest binding energy than 6DR were selected. Then, by examining the binding poses and non-covalent interactions, the top 10 compounds out of 100 were separated. Vina affinity is a Force-Field based Scoring Function, hence in order to validate and rescore the top 10 final compounds, we also used two scoring functions of X-Score (Empirical Scoring Functions) and DrugScore (Knowledge-Based Potentials) (Quiroga & Villarreal, 2016). In the end, 2 docked protein-ligand complexes with the best binding energy, X-Score, and DrugScore plus DfA1 complexes with TMP and 6DR were selected for comparison and further analyzes by MD simulation.

2.3. Molecular dynamics simulation and calculation of binding free energy

Although docking is a useful process in computational biology, it still has some flaws and since docking does not consider both ligand and protein to be flexible, MD simulation was performed to confirm the accuracy of the docking results. The topology parameters of DfrA1-DHFR were generated by Gromacs 5.1.4 package with CHARMM force field, whereas the topology parameters of hit compounds were generated by CHARMM general force field (CGENFF) web Server All of the studied complexes were placed in a triclinic box filled with TIP3P water model under periodic boundary condition (PBC). The neutralization of the systems was accomplished by adding Na^+ and Cl^- with a physiological NaCl concentration of 150mM. The energy minimization was done using the steepest descent method, then the 100ps NVT (constant number of particles, volume, and temperature) and 300ps NPT (constant number of particles, pressure, and temperature) were performed to equilibrate the system at 300 K and 1 bar. The Particle Mesh Ewald (PME) with 1.2 cut-off was used for the treatment of long-range electrostatic interactions (Aryapour et al., 2017; Sohraby, Bagheri, Aliyar, et al., 2017; Sohraby, Bagheri, Javaheri Moghadam, et al., 2017). Finally, the production run was performed for 150 ns.

The MD simulation results were analyzed by RMSD (Root-Mean-Square Deviation), RMSF (Root-Mean-Square fluctuation), the radius of gyration (Rg), and the number of H-bonds formed between the ligands and the protein. Also, the free binding energy of the protein and the hit compounds were estimated by the MM/PBSA (Molecular Mechanics Poisson Boltzmann Surface Area) method (Kollman et al., 2000; Miller et al., 2012; C. Wang et al., 2016). The general basis of this method is proportional to the following equation:

$$\Delta G_{bind} = G_{L.R} - G_L - G_R$$

Where $GL._R$, G_L, and G_R denote ligand-receptor complex, ligand, and protein, respectively. This method calculated the binding free energy, Van der Waals (VDW), and electrostatic energies of each protein-ligand trajectories (Kumari et al., 2014).

3. Results And Discussion

3.1. Docking

FDA-approved drugs data-set were docked toward DfrA1 by AutoDock Vina. The reference ligand (Fig. 1A) has the Vina affinity, X-score, and DrugScore of -8.7 Kcal/mol, 6.1, and − 48, respectively. In the first step, 100 compounds with the binding affinity lower than − 8.7 were selected. The full details information of these compounds are sorted in supplementary Table 1. After a careful analysis based on the binding poses and non-covalent interactions between the docked compound and DfrA1 active site residues, the top 10 compounds out of 100 were separated. Also, the number and residues involved in the hydrogen bond during docking were investigated, as shown in Table 2. Then, we rescored the top 10 compounds by X-score and DrugScore as shown in supplementary Table S2 (Table S2 was sorted based on X-score). The results of the two scorings were approximately the same as the results of the docking by Vina. The two compounds of the Olodaterol and Pazopanib which exhibited better Vina affinity, X-score, and DrugScore values than the reference ligand were selected as the hit compounds and their binding affinities were − 10.1, and − 9.8 kcal/mol, respectively (Fig. 1C-D). The Triamterene was excluded from the further investigation because of its low DrugScore, although its the Vina affinity and X-score was higher than the reference ligand (Table S2). Finally, trimethoprim (Fig. 1B) was individually docked with DfrA1 which gained the Vina affinity, X-score, and DrugScore of -5.1 Kcal/mol, 5.2 and − 25, respectively and indicating a decrease in the binding affinity of it compared to the reference ligand (Table 1). Lombardo *et al.*(Lombardo et al., 2016) showed that compound 17 with IC50 = 0.366 μM forms a conserved hydrogen bond with Glu 27. They also reported that compounds 17 and 3 have a hydrogen bond with Met 5. Interestingly in our study, Pazopanib, Olodaterol, and reference ligand have a conserved hydrogen bond with Glu 27 but this bond is not seen in the TMP-DfrA1 complex. On the other hand, due to the significant decrease in the binding affinity of trimethoprim, the H-bond between Glu 27 and inhibitors probably plays a critical role in inhibitors-DfrA1 connections.

3.2. MD simulation

3.2.1 The overall stability of DfrA1-ligand complexes

All of the DfrA1-ligand complexes (DfrA1-Pazopanib, DfrA1-Olodaterol, DfrA1-trimethoprim, and DfrA1-6DR) were simulated for the 150 ns by GROMACS to determine the affinity of the hit compounds and to analyze the flexibility and conformational changes.

In order to verify the conformational stability of the protein during 150 ns simulation, the backbone RMSD values of DfrA1 in the presence of the different ligands (Fig. 2A) were calculated. Also, the ligands fluctuation into the active site were monitored by RMSD in Fig. 2B separately. Besides, to provide a control to compare RMSD of the docked complexes, the crystal structure of DfrA1 with and without the 6DR was simulated. According to the protein RMSD curve, in the presence of 6DR, the mean RMSD extremely reduced and it reaches from 0.17 to 0.11 nm. As shown in Fig. 2B, the 6DR has maintained its position in the active site and equilibrated completely. In contrast to the reference inhibitor, the RMSD of

the DhfrA1 in the presence of TMP was increased from 0.06 nm at first to 0.25 nm at 130 ns and then it begins to decrease immediately. The TMP curve in the first 100 ns experiences an increase and decrease in RMSD. In the following, although this curve shows that TMP was equilibrated in the last 50 ns, the DfrA1 structure in the presence of TMP shows an increase of RMSD at the same time. The largest RMSD variation is related to Pazopanib. As shown in Fig. 2B, its RMSD has increased two times at 10 and 35 ns. After that its RMSD has decreased at 70 ns and equilibrated for 30 ns and then increased again. These widespread changes are due to the displacement of the Pazopanib structure shown in Fig. 5C. The RMSD curve of the Olodaterol shows that this compound has two small conformational changes at 15 and 32 ns. However, this movement has no major impact on the protein structure and it is more stable compared to the Pazopanib.

In the next step, to describe the flexibility and fluctuation of each residue Cα atom, the RMSF values of all protein-ligand complexes to the starting structures were calculated. The most fluctuations are related to N-terminal, C-terminal, and structural loops of protein including FG-loop, M20-loop, CD-loop, and loop 51–58 (Fig. 3A). As we expected, the highest mobility is related to the apo-protein and also the most fluctuation is observed in the M20-loop and CD-loop. The presence of 6DR in the active site has caused an extreme decrease in protein mobility, especially functional loops, including M20 and loop 51–58. These changes in the protein-trimethoprim complex are very small compared to the protein-6DR and it with the average RMSF of 0.096 nm has the closest fluctuation to the apo-protein, which is probably due to inappropriate interactions of TMP with active site residues. On the other hand, there is fluctuation decreasing in Pazopanib and Olodaterol. Although this decrease is not as much as the reference inhibitor, it is significant enough, especially in loops. In more detail, we have shown the fluctuation of the active site residues in Fig. 3B (Fig. 3B is just intended to better understand the conformational position of the active site residues in the apo form of DfrA1). The binding site residues showed different flexibilities in the presence and absence of ligands, it is demonstrated that these residues have essential interactions with ligand but the amount of these interactions are different and possibly as a result of ligands structural differences. For example, the Glu27 in DfrA1-6DR has a high fluctuation than other protein-ligand complexes and apo-protein. However, its other residues such as Met5, Ile20, Thr46, Met50, Leu53, and Ser96 have low flexibility than all other systems.

The radius of gyration was used to illustrate the level of compactness and its changes in the presence of the hit compounds. The Rg is defined as the mass-weighted root mean square distance of a collection of atoms from their common center of mass. The Rg values plots during the simulation time scale for apo-DfrA1 and the DfrA1-ligand complexes are shown in Fig. 3C. The apo-protein Rg values have a high fluctuation between 1.65 and 1.8 nm that shows it has a dynamic structure. The DfrA1-Pazopanib, DfrA1-Olodaterol, DfrA1-TMP, and DfrA1-6DR complexes have the average Rg of 1.56, 1.56, 1.57 and 1.55 nm, respectively, and show a lower Rg value than apo form. These values represent the structural stability and no significant conformational changes in the presence of the hit compounds during the simulation run. The data of these analyses suggest that ligands can stabilize conformation changes but the amount of stability is different and it probably depends on the enzyme's affinity for the compound and ligands structures.

The only contradiction is the high RMSD score of the Olodaterol and Pazopanib than TMP in the last 30ns which was due to the more frequent fluctuations of hits. Although Fig. 2B shows the high RMSD of the Olodaterol and Pazopanib in the last 30 ns but Fig. 3A clearly shows the structural equilibrium of the DfrA1-hit complexes at the same time. Moreover, the maximum RMSD values of all the systems after the equilibration state didn't exceed 0.3 nm and therefore the stability of the systems were evaluated for further analysis such as RMSF and Rg that these results show the stability of the systems too.

3.2.1 Ligand displacement and interactions analysis

The electrostatic interactions between protein and ligand such as hydrogen bond and salt bridge interactions have a critical role in protein-ligand stability and biological activity (Majewski et al., 2019). For this purpose, the hydrogen bond curve of protein and ligand was plotted for each system (Fig. 4). The reference ligand with a maximum of 8 hydrogen bonds has the highest interaction with the protein during the 150 ns simulation. Also, the least hydrogen bonds belong to trimethoprim, which is due to the lower stability of TMP in the active site of DfrA1. Two hit compounds of Pazopanib and Olodaterol have an acceptable number of hydrogen bonds during 150 ns simulation which shows that these hits have a stable conformation into the DfrA1 active site. However, the number of hydrogen bonds alone cannot indicate the affinity of an enzyme to a ligand. Accordingly, the DfrA1's interactions with each ligand were examined in detail. Since docking does not consider both ligand and protein to be flexible, we have used MD simulation to confirm the accuracy of the docking results. Here, the docked conformation of four compounds has been compared with the last frame of molecular dynamics simulation. As shown in Fig. 5A-D, except the reference inhibitor, the other ligands show conformation changes during simulation. 6DR as a crystallographic inhibitor of DfrA1 can form hydrogen bonds with residues Glu27 and the backbone carbonyl oxygen of Met5 through its pyrimidine 2 and 4 amino groups. The propargyl linker of 6DR forms π-π interactions with the nicotinamide group of NADPH to stabilize the protein-ligand complex. The Phe31 and Ile20 form key hydrophobic interactions with the propargyl linker of 6DR. Also, Phe31 has π-π stacking interaction with the pyrimidine ring. The phenyl and pyrimidine rings of 6DR have π-alkyl interaction with Met5 and Met50 side chains respectively. Additionally, Leu53 and Gln28 form π-sigma and π-donor hydrogen bond with pyridine ring of 6DR respectively (Fig. 5E). A remarkable point for the reference inhibitor is to maintain these interactions during the simulation. Conversely, TMP interactions with DfrA1 are limited and including hydrophobic interactions with Val6, Ala7, Ile20, Trp22, and Leu53 and also π-π and π-alkyl interactions of Phe31and Met50 with the pyrimidine and phenyl ring respectively. The TMP forms hydrogen bonds with some active site residues such as Thr47, Ser49, and Pro18 in some frames of the simulation but as previously mentioned, the number of hydrogen bonds alone cannot indicate the affinity of an enzyme to a ligand. For example, TMP does not form any hydrogen bonds with the essential residues of the active site like Glu27. Additionally, in the resistant enzyme, Leu 28 replaced with Gln which in current study Gln28 has no interaction with TMP (Fig. 5F).

The interactions of hit compounds are very similar to the reference inhibitor. For example, Tyr102 and Met5 have two hydrogen bonds with the Benzoxazine hydroxyl moiety of Olodaterol and Also, Glu27 forms a salt bridge with the Benzoxazine amine moiety. This salt bridge also observed in Glu27 and

sulfonamide group of Pazopanib which shows the vital role of Glu27 in inhibition of DfrA1 by small molecules. Besides, Pazopanib can form two hydrogen bonds with Ile20 and Trp22. Phe31 in both hits form π-π interactions with inhibitor rings (Fig. 5G-H). All of these features suggest that Pazopanib and Olodaterol can be an effective ligand for DfrA1 cavity.

3.2.2 Binding free energy

To quantify the binding affinity of hit compounds to DfrA1, the binding free energies of two hits were predicted by MM-PBSA method. As shown in Table 3, the values of the van der Waals energy of the Olodaterol and Pazopanib plus 6DR and trimethoprim were − 210.4 kcal/mol, − 347.6 kcal/mol, − 188.9 kcal/mol, and − 238.2 kcal/mol, respectively. It is shown that the binding pocket of the DfrA1 is mainly composed of hydrophobic residues such as Met5, Val6, Ala7, Ile20, Trp22, Phe31, Met50, and Leu53. Also, the calculated electrostatic interactions for all of the complexes, except for Trimrthorime, were approximately close to each other, ranging from − 445.5 to − 532.6 kcal/mol. This was probably because the hydrogen-bonding interactions in the three complexes (Olodaterol and Pazopanib, and 6DR) are similar. This issue also demonstrates the importance of hydrogen bonds in enhancing the binding affinity of the inhibitors to DfrA1. The reference ligand has higher electrostatic interactions than the Olodaterol and Pazopanib which is probably due to the number (four H-bonds) and residues (Met5, Glu27, Leu32, Tyr102) involved in its hydrogen bonds.

In the Trimethorime-DfrA1 complex, the electrostatic interaction (− 334.8 kcal/mol) slightly cooperated to the binding of the inhibitors as compared with the other three complexes. This large difference might reflect that the hydrogen bond between the TMP moiety and the DfrA1 active site residues (Ser49) were not essentially stabilizing interaction to those hydrogen bonds with other residues observed in the other three complexes, such as Glu27. The above data shows that both the van der Waals and electrostatic interactions play key roles in the activities of these compounds. On the other hand, the Olodaterol, 6DR, Pazopanib, and TMP have ΔGbind − 365, -284, -28 and 9.8 Kcal/mol, respectively. These results indicate that Olodaterol has greater free binding energy as compared to reference ligand but the Pazopanib and TMP showed less binding energy as compared to it. As expected, the MM/PBSA data is almost in line with the docking data. For example, trimethoprim received van der Waals, electrostatic interactions, and binding free energy much lower than the reference inhibitor and two other compounds and while Pazopanib has low binding free energy (-28) and very high electrostatic energy (-485.7). Taken together, data from this method, along with molecular docking as well as analyzes performed during molecular dynamics simulations, suggest that our hit compounds have the potential to significantly bind and inhibit trimethoprim-resistant dihydrofolate reductase.

4. Conclusion

Klebsiella pneumoniae is a pathogenic bacterium that has a strong resistance to antibiotics, as far as the World Health Organization identifies it as one of the greatest threats to human health. A major target in this infectious bacterium for drug design is the dihydrofolate reductase. This enzyme is resistant to trimethoprim by several mutations in essential active site residues. In this study, we used a structure-

based screening and MD simulation and MM/PBSA to identify new inhibitors for the Kp-DfrA1. They showed that DfrA1-hit (Olodaterol and Pazopanib) complexes are more stable compared with the apo-protein and DfrA1-trimethoprim complex. During this study, the hit compounds' results were compared with reference ligand and trimethoprim as positive and negative controls, respectively. According to the results of this study, the Olodaterol and Pazopanib can be potent inhibitors for K. pneumoniae trimethoprim-Resistant dihydrofolate reductase. Investigation of different parts of this research including docking, MD simulation, and MM/PBSA shows the correlation between results. However, if there are any contradictions, probably due to molecular docking that still faces a lot of challenges, especially for efficiently exploring the conformational space of target proteins and ligands and developing scoring functions to estimate the free energies of protein-ligand binding. Also, one of the biggest challenges in Structure-Based Drug Design (SBDD) methods is the target's flexibility. Docking software provides sufficient flexibility for the ligands but they have a big limitation to supply the receptor flexibility. With all these limitations, there is a very large list of novel and potent drug developed by SBDD. Some of the successful drug repositioning and SBDD examples are the Prostaglandin E2, Leflunomide a pyrimidine biosynthesis inhibitor, and NRB04248 a very potent inhibitor of Mycobacterium tuberculosis (This compound can inhibit Mycobacterium tuberculosis without any cytotoxic effects against host cells). These successes demonstrate the high efficiency of computational methods. On the other hand, to confirm the docking results of AutoDock Vina, also, we used two different type scoring functions of Empirical Scoring Functions and Knowledge-Based Potentials. Since in this study, the potential inhibitors were selected by the drug repurposing method and the Olodaterol and Pazopanib were the FDA-approved drugs and their toxicity profiles have known, so we can evaluate theirs in phase 2 clinical trials. This method speeds up the design and discovery process of the drugs and greatly reduces its cost.

Declarations

Funding:

No funding to declare. This research received no specific grant from any funding agency in the public, commercial, or not-for-profit sectors.

Availability of data and material:

The authors confirm that the data supporting the findings of this study are available within the article and supplementary materials.

Code availability:

Not applicable

Author contributions

Mostafa Khedrinia: Conceptualization, Investigation, Methodology, Writing-original draft

Farzad Khademi: Methodology, Data curation, Writing-review and editing

Seyed Ali Mirhosseini: Investigation, Data curation, Writing-review and editing

Ramezan Ali Taheri: Conceptualization, Supervision, Writing-review and editing

Conflicts of interest/Competing interests:

The authors confirm that they have no conflict of interest.

Acknowledgment:

Thanks to guidance and advice from "Clinical Research Development Unit of Baqiyatallah Hospital".

References

1. Anderson, A. C. (2005). Targeting DHFR in parasitic protozoa. *Drug Discovery Today*, *10*(2), 121–128. https://doi.org/10.1016/S1359-6446(04)03308-2
2. Aryapour, H., Dehdab, M., Sohraby, F., & Bargahi, A. (2017). Prediction of new chromene-based inhibitors of tubulin using structure-based virtual screening and molecular dynamics simulation methods. *Comput. Biol. Chem*, *71*, 89–97. https://doi.org/10.1016/j.compbiolchem.2017.09.007
3. Bastos, L. D. C., de Souza, F. R., Guimarães, A. P., Sirouspour, M., Cuya Guizado, T. R., Forgione, P., Ramalho, T. C., & França, T. C. C. (2016). Virtual screening, docking, and dynamics of potential new inhibitors of dihydrofolate reductase from Yersinia pestis. *Journal of Biomolecular Structure and Dynamics*, *34*(10), 2184–2198. https://doi.org/10.1080/07391102.2015.1110832
4. Batool, M., Ahmad, B., & Choi, S. (2019). A Structure-Based Drug Discovery Paradigm. *Int. J. Mol. Sci.*, *20*(11), 2783. https://doi.org/10.3390/ijms20112783
5. Brisse, S., Milatovic, D., Fluit, a D. C., Verhoef, J. a N., Martin, N., Scheuring, S., Köhrer, K., & Schmitz, F.-J. (1999). Comparative In Vitro Activities of Ciprofloxacin , Clinafloxacin , Gatifloxacin , Levofloxacin , Moxifloxacin , and Trovafloxacin against Klebsiella pneunoniae, Klebsiella oytoca, Enterobacter cloacae and Enterobacter aerogenes Clinical Isolates with Alte. *Society*, *43*(8), 2051–2055.
6. Brolund, A., Sundqvist, M., Kahlmeter, G., & Grape, M. (2010). Molecular characterisation of trimethoprim resistance in Escherichia coli and Klebsiella pneumoniae during a two year intervention on trimethoprim use. *PLoS ONE*, *5*(2), 1–5. https://doi.org/10.1371/journal.pone.0009233
7. Capoor, M. R., Nair, D., Rajni, Khanna, G., Krishna, S. V, Chintamani, M. S., & Aggarwal, P. (2008). Microflora of bile aspirates in patients with acute cholecystitis with or without cholelithiasis: a tropical experience. *The Brazilian Journal of Infectious Diseases : An Official Publication of the Brazilian Society of Infectious Diseases*, *12*(3), 222–225. https://doi.org/http://dx.doi.org/10.1590/S1413-86702008000300012
8. Chung, P. Y. (2016). The emerging problems of Klebsiella pneumoniae infections: Carbapenem resistance and biofilm formation. *FEMS Microbiology Letters*, *363*(20), 1–6.

https://doi.org/10.1093/femsle/fnw219

9. Doorduijn, D. J., Rooijakkers, S. H. M., van Schaik, W., & Bardoel, B. W. (2016). Complement resistance mechanisms of Klebsiella pneumoniae. *Immunobiology*, *221*(10), 1102–1109. https://doi.org/10.1016/j.imbio.2016.06.014
10. El Bouamri, M. C., Arsalane, L., El Kamouni, Y., & Zouhair, S. (2015). Antimicrobial susceptibility of urinary Klebsiella pneumoniae and the emergence of carbapenem-resistant strains: A retrospective study from a university hospital in Morocco, North Africa. *African Journal of Urology*, *21*(1), 36–40. https://doi.org/10.1016/j.afju.2014.10.004
11. Fang, C. T., Chen, Y. C., Chang, S. C., Sau, W. Y., & Luh, K. T. (2000). Klebsiella pneumoniae meningitis: timing of antimicrobial therapy and prognosis. *QJM: Monthly Journal of the Association of Physicians*, *93*(1), 45–53. https://doi.org/10.1093/qjmed/93.1.45
12. Girometti, N., Lewis, R. E., Giannella, M., Ambretti, S., Bartoletti, M., Tedeschi, S., Tumietto, F., Cristini, F., Trapani, F., Gaibani, P., & Viale, P. (2014). Klebsiella pneumoniae bloodstream infection epidemiology and impact of inappropriate empirical therapy. *Medicine (United States)*, *93*(17), 298–308. https://doi.org/10.1097/MD.0000000000000111
13. Gohlke, H., Hendlich, M., & Klebe, G. (2000). Knowledge-based scoring function to predict protein-ligand interactions. *Journal of Molecular Biology*, *295*(2), 337–356. https://doi.org/10.1006/jmbi.1999.3371
14. Gordin, F. M. (1984). Adverse Reactions to Trimethoprim-Sulfamethoxazole in Patients with the Acquired Immunodeficiency Syndrome. *Annals of Internal Medicine*, *100*(4), 495. https://doi.org/10.7326/0003-4819-100-4-495
15. Hawser, S. P., Bouchillon, S. K., Lascols, C., Hackel, M., Hoban, D. J., Badal, R. E., Woodford, N., & Livermore, D. M. (2011). Susceptibility of Klebsiella pneumoniae isolates from intra-abdominal infections and molecular characterization of ertapenem-resistant isolates. *Antimicrobial Agents and Chemotherapy*, *55*(8), 3917–3921. https://doi.org/10.1128/AAC.00070-11
16. Hirsch, E. B., Chang, K. T., Lasco, T. M., Caeiro, J. P., & Tam, V. H. (2011). Emergence of KPC-producing Klebsiella pneumoniae in Texas. *Diagnostic Microbiology and Infectious Disease*, *69*(2), 234–235. https://doi.org/10.1016/j.diagmicrobio.2010.09.003
17. Ho, J. M. W., & Juurlink, D. N. (2011). Considerations when prescribing trimethoprim-sulfamethoxazole. *Cmaj*, *183*(16), 1851–1858. https://doi.org/10.1503/cmaj.111152
18. Hoffman, a. M., Viel, L., Muckle, C. a., Yager, J. S., & Staempfli, H. R. (1992). Evaluation of sulbactam plus ampicillin for treatment of experimentally induced Klebsiella pneumoniae lung infection in foals. *American Journal of Veterinary Research*, *53*(6), 1059–1067.
19. Kidd, T. J., Mills, G., Sá-Pessoa, J., Dumigan, A., Frank, C. G., Insua, J. L., Ingram, R., Hobley, L., & Bengoechea, J. a. (2017). A *Klebsiella pneumoniae* antibiotic resistance mechanism that subdues host defences and promotes virulence. *EMBO Molecular Medicine*, *9*(4), 430–447. https://doi.org/10.15252/emmm.201607336

20. Kollman, P. A., Massova, I., Reyes, C., Kuhn, B., Huo, S., Chong, L., Lee, M., Lee, T., Duan, Y., Wang, W., Donini, O., Cieplak, P., Srinivasan, J., Case, D. A., & Cheatham, T. E. (2000). Calculating structures and free energies of complex molecules: Combining molecular mechanics and continuum models. *Accounts of Chemical Research*, *33*(12), 889–897. https://doi.org/10.1021/ar000033j
21. Kubbies, M., & Stockinger, H. (1990). Cell cycle-dependent DHFR and t-PA production in cotransfected, MTX-amplified CHO cells revealed by dual-laser flow cytometry. *Experimental Cell Research*, *188*(2), 267–271. https://doi.org/10.1016/0014-4827(90)90169-B
22. Kumari, R., Kumar, R., & Lynn, A. (2014). G-mmpbsa -A GROMACS tool for high-throughput MM-PBSA calculations. *Journal of Chemical Information and Modeling*, *54*(7), 1951–1962. https://doi.org/10.1021/ci500020m
23. Lam, T., Hilgers, M. T., Cunningham, M. L., Kwan, B. P., Nelson, K. J., Brown-Driver, V., Ong, V., Trzoss, M., Hough, G., Shaw, K. J., & Finn, J. (2014). Structure-based design of new dihydrofolate reductase antibacterial agents: 7-(benzimidazol-1-yl)-2,4-diaminoquinazolines. *Journal of Medicinal Chemistry*, *57*(3), 651–668. https://doi.org/10.1021/jm401204g
24. Lamb, K. M., Lombardo, M. N., Alverson, J., Priestley, N. D., Wright, D. L., & Anderson, A. C. (2014). Crystal structures of klebsiella pneumoniae dihydrofolate reductase bound to propargyl-linked antifolates reveal features for potency and selectivity. *Antimicrobial Agents and Chemotherapy*, *58*(12), 7484–7491. https://doi.org/10.1128/AAC.03555-14
25. Li, B., Zhao, Y., Liu, C., Chen, Z., & Zhou, D. (2014). Molecular pathogenesis of *Klebsiella pneumoniae*. *Future Microbiology*, *9*(9), 1071–1081. https://doi.org/10.2217/fmb.14.48
26. Lombardo, M. N., G-Dayanandan, N., Wright, D. L., & Anderson, A. C. (2016). Crystal Structures of Trimethoprim-Resistant DfrA1 Rationalize Potent Inhibition by Propargyl-Linked Antifolates. *ACS Infectious Diseases*, *2*(2), 149–156. https://doi.org/10.1021/acsinfecdis.5b00129
27. Maffiolo, C., Novellas, S., Chevallier, P., Brunner, P., Mourou, M. Y., & Bruneton, J. N. (2006). Thrombophlebitis of the hepatic veins: Complication of a Klebsiella liver abscess. *Clinical Imaging*, *30*(1), 63–65. https://doi.org/10.1016/j.clinimag.2005.07.021
28. Majewski, M., Ruiz-Carmona, S., & Barril, X. (2019). An investigation of structural stability in protein-ligand complexes reveals the balance between order and disorder. *Communications Chemistry*, *2*(1). https://doi.org/10.1038/s42004-019-0205-5
29. Miller, B. R., McGee, T. D., Swails, J. M., Homeyer, N., Gohlke, H., & Roitberg, A. E. (2012). MMPBSA.py: An efficient program for end-state free energy calculations. *Journal of Chemical Theory and Computation*, *8*(9), 3314–3321. https://doi.org/10.1021/ct300418h
30. Munita, J. M., Arias, C. a, Unit, A. R., & Santiago, A. De. (2016). Mechanisms of Antibiotic Resistance. *Microbiol Spectr*, *4*(2), 1–37. https://doi.org/10.1128/microbiolspec.VMBF-0016-2015.Mechanisms
31. Naveja, J. J., Dueñas-gonzález, A., & Medina-franco, J. L. (2011). Drug Repurposing for Epigenetic Targets Guided by Computational Methods. In *Epi-Informatics*. Elsevier Inc. https://doi.org/10.1016/B978-0-12-802808-7.00012-5

32. Navon-Venezia, S., Kondratyeva, K., & Carattoli, A. (2017). Klebsiella pneumoniae: A major worldwide source and shuttle for antibiotic resistance. *FEMS Microbiology Reviews*, *41*(3), 252–275. https://doi.org/10.1093/femsre/fux013
33. Nickels, L. C., Jones, C., & Stead, L. G. (2012). Trimethoprim-sulfamethoxazole-induced hyperkalemia in a patient with normal renal function . *Case Reports in Emergency Medicine* , *2012* , 815907. https://doi.org/10.1155/2012/815907
34. Pacheco Homem, D., Flores, R., Tosqui, P., De Castro Rozada, T., Abicht Basso, E., Gasparotto Junior, A., & Augusto Vicente Seixas, F. (2013). Homology modeling of dihydrofolate reductase from T. gondii bonded to antagonists: Molecular docking and molecular dynamics simulations. *Molecular BioSystems*, *9*(6), 1308–1315. https://doi.org/10.1039/c3mb25530a
35. Prince, S. E., Dominger, K. A., Cunha, B. A., Klein, N. C., Brook, M., Brook, S. (2000). - Klebsiella pneumoniae: Pneumonia. - *Clinical Pulmonary Medicine*, *7*(6), 295–303. https://doi.org/10.1016/S0147-9563(97)90028-5
36. Quiroga, R., & Villarreal, M. a. (2016). Vinardo: A scoring function based on autodock vina improves scoring, docking, and virtual screening. *PLoS ONE*, *11*(5), 1–18. https://doi.org/10.1371/journal.pone.0155183
37. Rana, R. M., Rampogu, S., Zeb, A., Son, M., Park, C., Lee, G., Yoon, S., Baek, A., Parameswaran, S., Park, S. J., & Lee, K. W. (2019). In Silico Study Probes Potential Inhibitors of Human Dihydrofolate Reductase for Cancer Therapeutics. *Journal of Clinical Medicine*, *8*(2), 233. https://doi.org/10.3390/jcm8020233
38. Rao, A. S., & Road, K. (2013). A study on dyhydrofolate reductase and its inhibitors: a review. *International J*, *4*(7), 2535–2547. https://doi.org/10.13040/IJPSR.0975-8232.4(7).2535-47
39. Rijal, J. P., Pompa, T., Giri, S., & Raj Bhatt, V. (2014). A case of toxic epidermal necrolysis caused by trimethoprim- sulfamethoxazole. *BMJ Case Reports*, 2–4. https://doi.org/10.1136/bcr-2013-203163
40. Sanders, J. a. (1989). Klebsilla Pneumoniae Osteomylitis: Demonastration by Three-Phase Radionuclide Bone Imaging. *J Nucl Med*, *30*, 1412–1414.
41. Sohraby, F., Bagheri, M., Aliyar, M., & Aryapour, H. (2017). In silico drug repurposing of FDA-approved drugs to predict new inhibitors for drug resistant T315I mutant and wild-type BCR-ABL1: A virtual screening and molecular dynamics study. *Journal of Molecular Graphics and Modelling*, *74*, 234–240. https://doi.org/10.1016/j.jmgm.2017.04.005
42. Sohraby, F., Bagheri, M., Javaheri Moghadam, M., & Aryapour, H. (2017). In silico prediction of new inhibitors for the nucleotide pool sanitizing enzyme, MTH1, using drug repurposing. *Journal of Biomolecular Structure and Dynamics*, *1102*(September), 1–9. https://doi.org/10.1080/07391102.2017.1365013
43. Vadloori, B., Sharath, a. K., Prabhu, N. P., & Maurya, R. (2018). Homology modelling, molecular docking, and molecular dynamics simulations reveal the inhibition of Leishmania donovani dihydrofolate reductase-thymidylate synthase enzyme by Withaferin-A. *BMC Research Notes*, *11*(1), 1–7. https://doi.org/10.1186/s13104-018-3354-1

44. Velázquez, H., Perazella, M. a., Wright, F. S., & Ellison, D. H. (1993). Renal mechanism of trimethoprim-induced hyperkalemia. *Annals of Internal Medicine*, *119*(4), 296–301. https://doi.org/10.7326/0003-4819-119-4-199308150-00008
45. Wang, C., Nguyen, P. H., Pham, K., Huynh, D., Le, T. B. N., Wang, H., Ren, P., & Luo, R. (2016). Calculating protein–ligand binding affinities with MMPBSA: Method and error analysis. *Journal of Computational Chemistry*, 2436–2446. https://doi.org/10.1002/jcc.24467
46. Wang, H., Zhang, C., Feng, J., Liu, Y., Yang, Q., Chen, H., Gu, Z., Zhang, H., Chen, W., & Chen, Y. Q. (2016). Role of dihydrofolate reductase in tetrahydrobiopterin biosynthesis and lipid metabolism in the oleaginous fungus Mortierella alpina. *Microbiology (United Kingdom)*, *162*(9), 1544–1553. https://doi.org/10.1099/mic.0.000345
47. Wu, W., Jin, Y., Bai, F., & Jin, S. (2015). Pseudomonas aeruginosa. *Molecular Medical Microbiology*, *163*, 753–767. https://doi.org/10.1016/B978-0-12-397169-2.00041-X

Tables

Table 1. Results of molecular docking scores, x-score and DrugScore of two hit compounds plus 6DR and TMP inside the binding site of DfrA1.

Hit compounds	Vina affinity (kcal/mol)	X-score	DrugScore	Categories
Pazopanib	-10.1	7.4	-63	Kinase inhibitor
Olodaterol	-9.8	7.8	-55	Adrenergic agents
6DR	-8.7	6.1	-48	DfrA1 inhibitor
Trimethoprim	-5.1	5.2	-25	DHFR inhibitor

Table 2. Results of interacting residues and the number of hydrogen bonds with protein-ligand complexes after docking.

Ligand–enzyme complex	Interacting residues	No. of H-bonds
DfrA1-6DR	Met5, Glu27, Lys32, Tyr102	4
DfrA1-Olodaterol	Met5, Glu27, Glu27	3
DfrA1-Pazopanib	Ile20, Trp22, Glu27	3
DfrA1-TMP	Ser49, Ser49	2

Table 3. VDW, Electrostatic, and binding free energies of the hit compounds in complex with Trimethoprim-resistant dihydrofolate reductase. All values were calculated as kJ/mol.

Hit names	van der Waals energy	Electrostatic energy	Binding free energy
Olodaterol	-210.4 ± 5	-445.5 ± 10	-365.2 ± 6
6DR	-347.6 ± 9	-532.6 ± 15.3	-284.5 ± 10
Pazopanib	-188.9 ± 11	-485.7 ± 13.8	-28 ± 13
Trimrthorime	-238.2 ± 7	-334.8 ± 11.4	9.8 ± 5

Figures

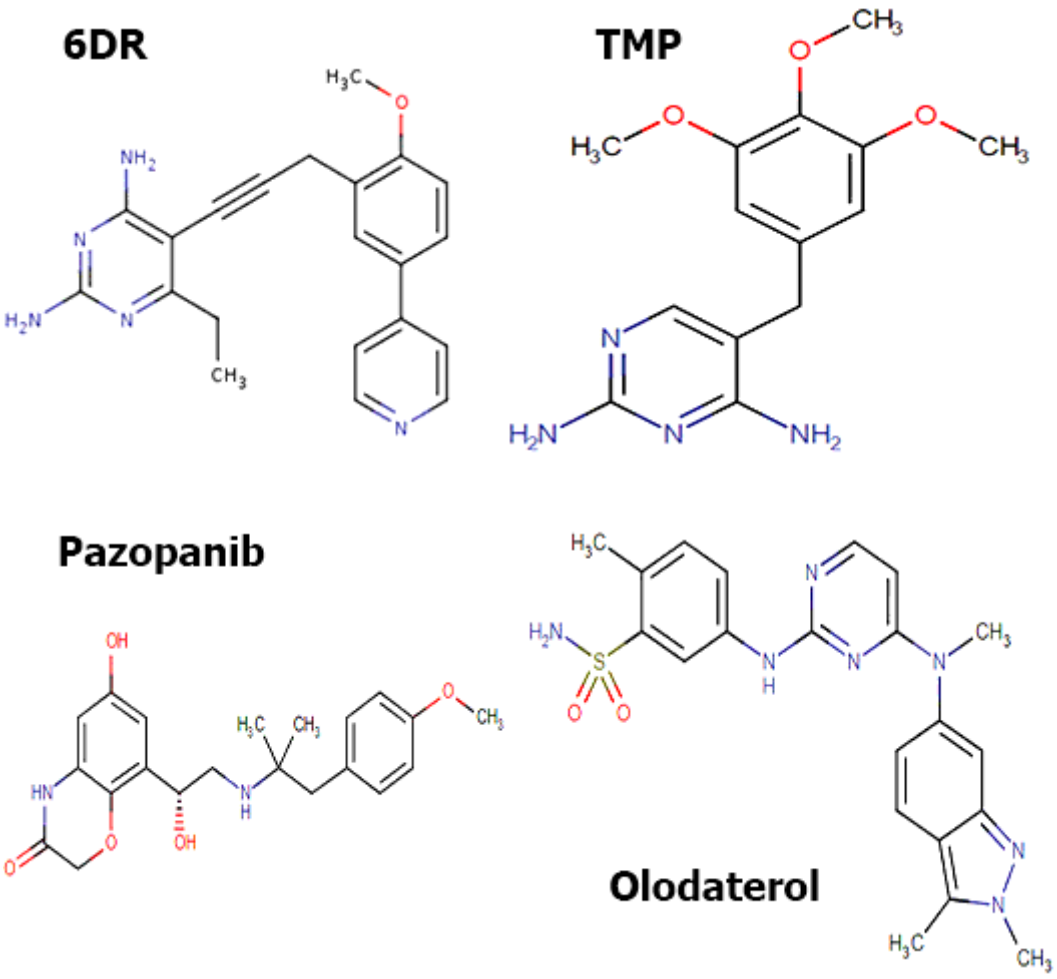

Figure 1

The 2D chemical structures of reference ligand, TMP and the best ligands from molecular docking simulation. (A) 6DR, (B) Trimethoprim, (C) Olodaterol and (D) Pazopanib.

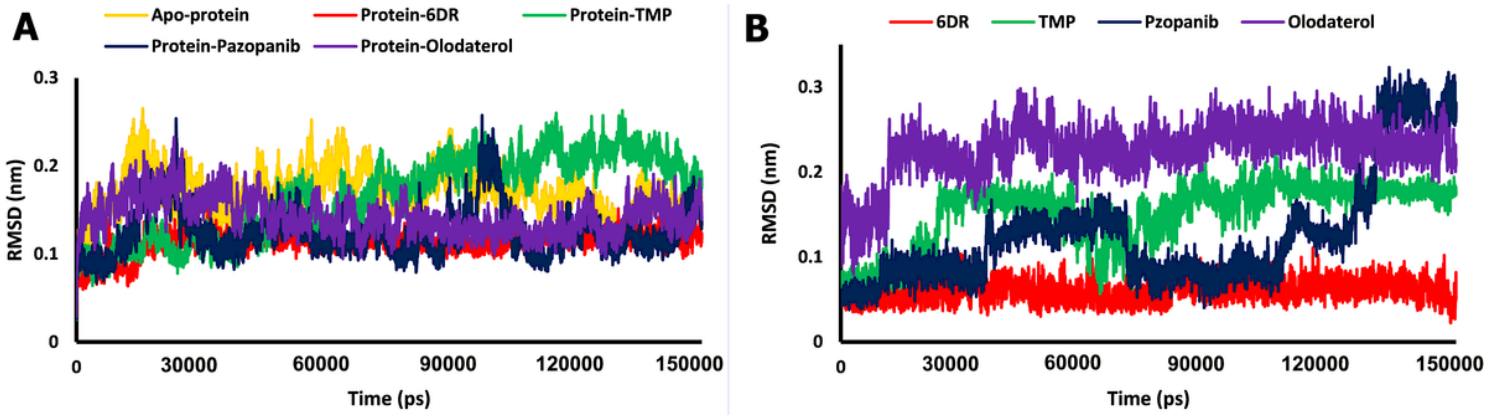

Figure 2

The backbone RMSD of apo-protein and DfrA1-ligands (A), and only ligand RMSD (B) during 150 ns MD simulations.

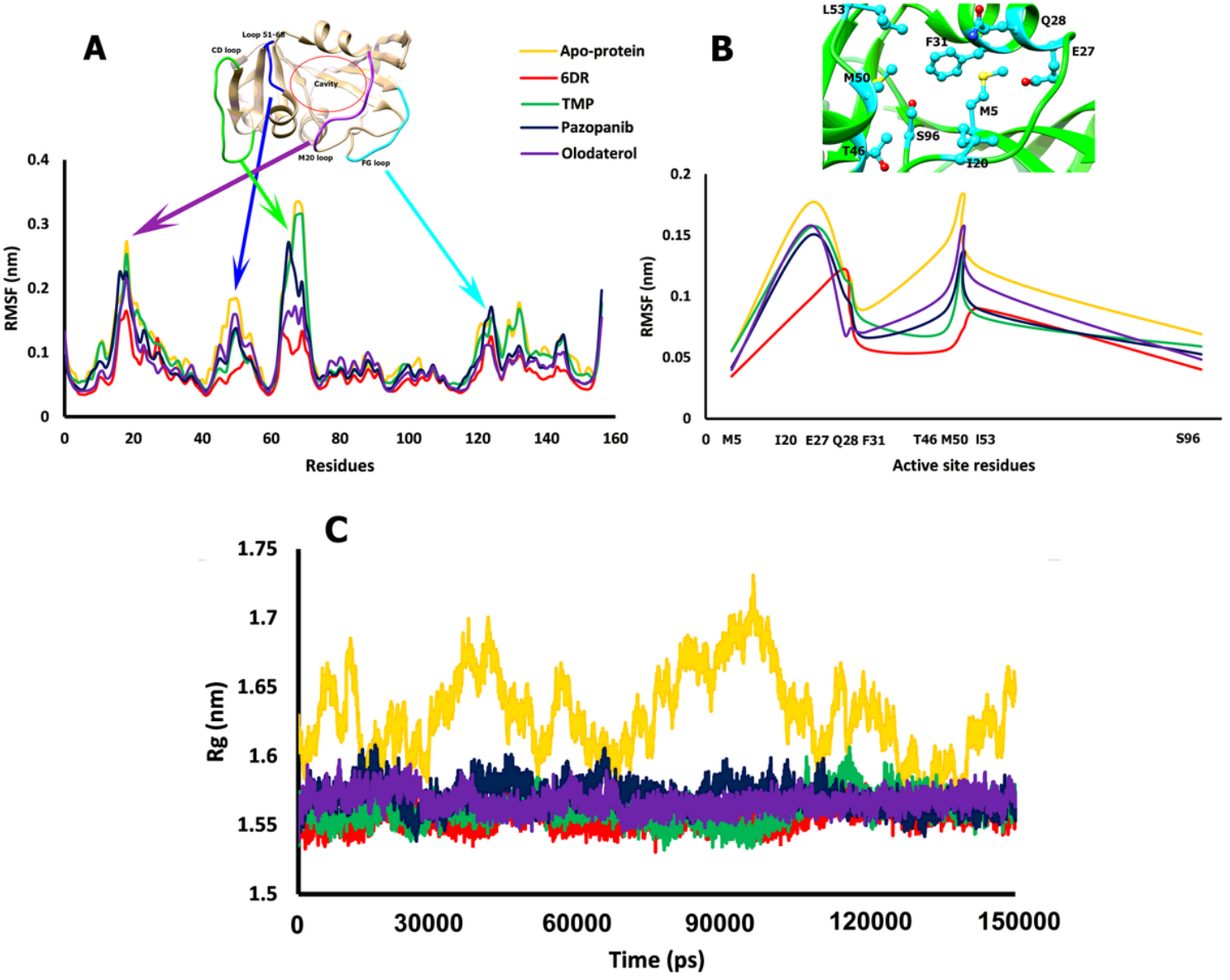

Figure 3

The Ca atoms RMSF of apo-protein and DfrA1 in complex with ligands (A), The active site key residues RMSF (B) and the backbone radius of gyration versus time plot for DfrA1-ligand complexes compared to apo-protein (C) during 150 ns MD simulation.

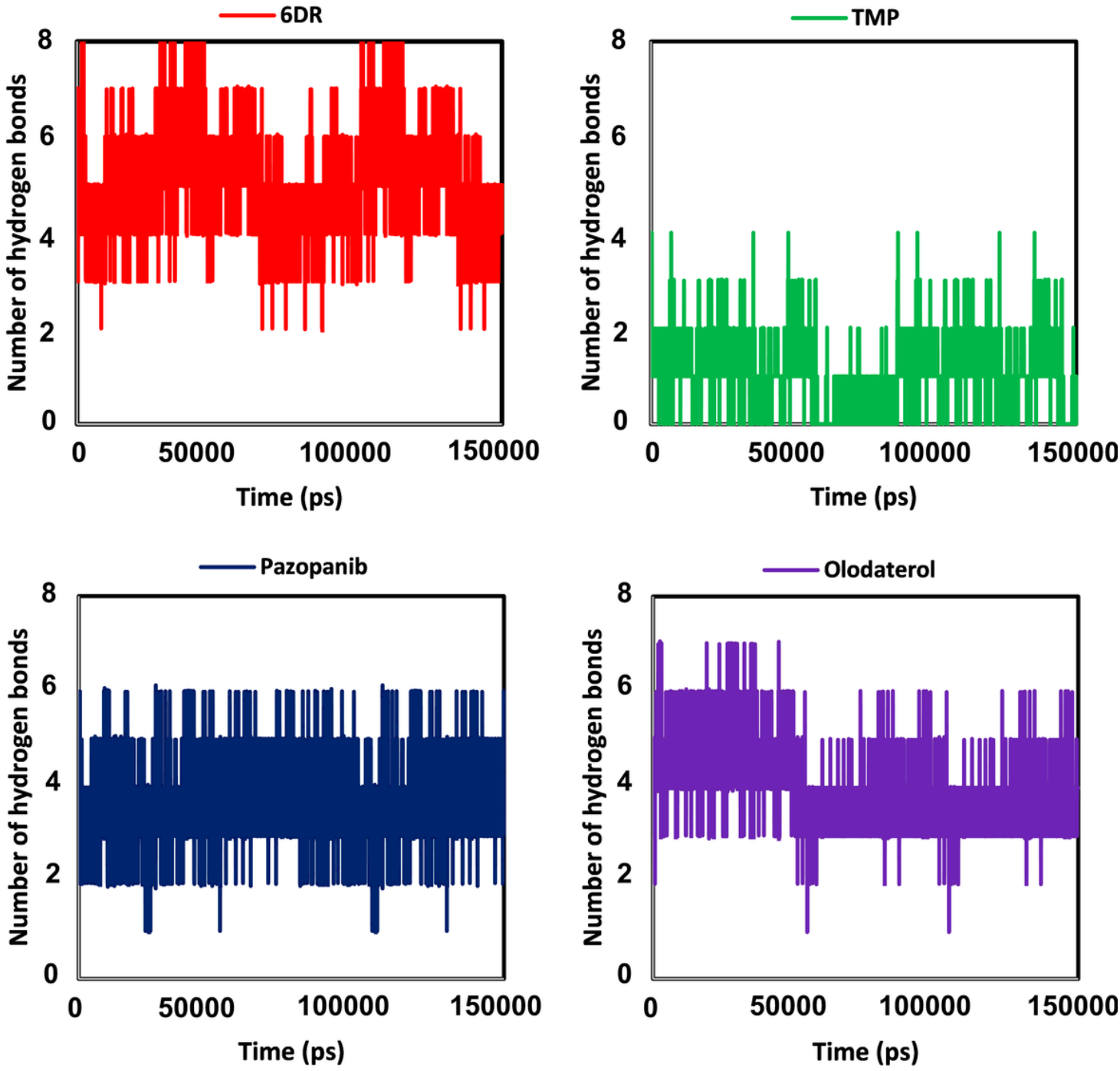

Figure 4

The number of hydrogen bonds between ligands and the residues of the active site of DfrA1.

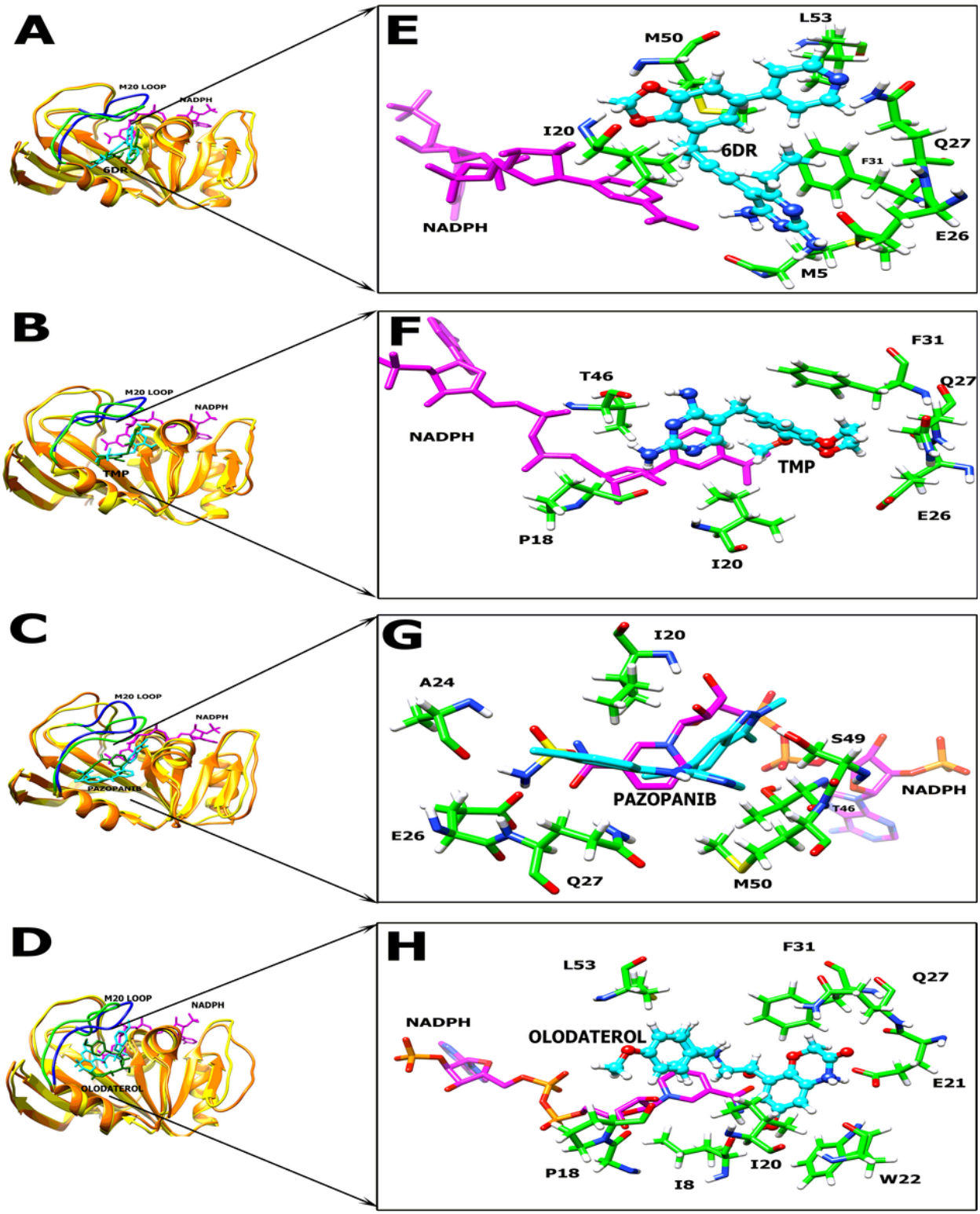

Figure 5

The 3D structures of the protein-ligand complexes (A-D) and essential residues (E-H) in the active site of DfrA1, (A) 6DR, (B) TMP, (C) Olodaterol and (D) Pazopanib.

Supplementary Files

This is a list of supplementary files associated with this preprint. Click to download.

- KhedriniaTableS1.docx
- KhedriniaTableS2.docx